

Materials Research Society Spring Meeting

San Francisco, CA; April 13-17, 1998

SYMPOSIUM W Rapid Thermal and Integrated Processing VII

Chairs: M. Ozturk, S. Pas, F. Roozeboom, P. Timans

(invited)

SIMULATION OF RAPID THERMAL ANNEALED BORON ULTRA-SHALLOW JUNCTIONS IN INERT AND OXIDIZING AMBIENT

W. LERCH¹, M. GLÜCK¹, N. A. STOLWIJK², H. WALK^{1,3}, M. SCHÄFER³, S. D. MARCUS⁴,
D. F. DOWNEY⁵, J. W. CHOW⁵, H. MARQUARDT⁶

¹ STEAG AST Elektronik GmbH, Dornstadt, Germany, W.LERCH@STEAG-AST.DE

² Institut für Metallforschung, Westfälische Wilhelms-Universität Münster, Germany

³ CADwalk, Allmendingen, Germany

⁴ STEAG AST Elektronik, Tempe (AZ), USA

⁵ Varian Ion Implant Systems, Gloucester (MA), USA,

⁶ Silvaco Data Systems, Munich, Germany

Proceedings published as Volume 525 of the Materials Research Society Symposium Proceedings Series.

SIMULATION OF RAPID THERMAL ANNEALED BORON ULTRA-SHALLOW JUNCTIONS IN INERT AND OXIDIZING AMBIENT

W. LERCH¹, M. GLÜCK¹, N. A. STOLWIJK², H. WALK^{1,3}, M. SCHÄFER³, S. D. MARCUS⁴,
D. F. DOWNEY⁵, J. W. CHOW⁵, H. MARQUARDT⁶

¹ STEAG AST Elektronik GmbH, Dornstadt, Germany, W.LERCH@STEAG-AST.DE

² Institut für Metallforschung, Westfälische Wilhelms-Universität Münster, Germany

³ CADwalk, Allmendingen, Germany

⁴ STEAG AST Elektronik, Tempe (AZ), USA

⁵ Varian Ion Implant Systems, Gloucester (MA), USA,

⁶ Silvaco Data Systems, Munich, Germany

ABSTRACT

Rapid Thermal Annealing (RTA) is indispensable for the formation of ultra-shallow source/drain junctions. To improve the annealing conditions, a fundamental understanding of the influences on the diffusion/activation process is necessary. Ion implantations of 1 keV boron at a dose of $\Phi \approx 1 \cdot 10^{15} \text{ cm}^{-2}$ are annealed in a SHS2800e RTP-system under controlled concentrations of oxygen in nitrogen ambient (0-1 ppm up to 1%). Concentration-depth profiles, measured by Secondary Ion Mass Spectroscopy (SIMS), are simulated within the framework of the kick-out model involving diffusion enhancement via supersaturation of silicon self-interstitials. The validity of this interpretation is supported by the simulated results which are in good agreement with experimental data. After RTA for 10 s at 1050°C the junctions are varying within a range of 800 Å to 1400 Å depending on the annealing ambient. The results of the simulation yield finite values of self-interstitial supersaturation as a function of the oxygen concentration.

INTRODUCTION

With the continuous down-scaling of all relevant device parameters in silicon ULSI technology and the increasing circuit complexity, long-time furnace annealing steps have gradually been replaced by RTP processes in the critical section of the device fabrication process [1]. One of the main technological challenges is the formation of shallow source and drain junctions with low parasitic series resistance in conjunction with deeper, heavily doped contact regions for low-leakage self-aligned silicide contacts and minimized short-channel effects. According to the National Technology Roadmap for Semiconductors (NTRS), these will be in the order of a few tens of nanometers for the up-coming 0.18 and 0.13 μm circuit generations. Low energy implants (As, P for n-type and B, BF₂ for p-type, respectively) are commonly used. Numerous publications

from our laboratories (STEAG AST Elektronik GmbH, VARIAN IIS) have already focused on techniques and processing conditions to produce ultra-shallow junctions [2, 3, 4, 5, 6]. Based on the current and previous works, a patent pending process using controlled low ppm levels of O₂ for the creation of ultra-shallow junctions has been developed [7].

It is currently projected that 0.07 μm technology will require junction depths of about 300 Å [8]. This has an important impact on the amount of Transient Enhanced Diffusion (TED), which can be tolerated. A fundamental understanding of TED and oxidation enhanced diffusion (OED) effects, which both affect junction depth, is essential [9]. The TED is inevitable and causes enhanced diffusion being several orders of magnitude higher than intrinsic values. This is due to the generation of excess self-interstitials in the form of single self-interstitials, self-clusters and dopant-interstitial clusters during ion implantation [10]. Several previous studies have already reported anomalous diffusion behaviors in the presence of point-defect concentrations in excess of their equilibrium values [11, 12, 13, 14, 15].

Oxidation during annealing is known to perturb the point defect concentrations by generating excess self-interstitials. They tend to enhance the diffusivities of dopant atoms which diffuse with a significant interstitialcy component (e.g. boron) and to retard diffusivities of atoms which predominantly diffuse via vacancies (e.g. arsenic, antimony) [11, 12, 16]. The effect of pure nitrogen annealing ambient, present in the reactor chamber, has previously been reported [16].

With the experiments [17] and the actual follow-up simulations we intend to study the diffusion mechanism and the influence of the gaseous ambient during annealing (e. g. 1050°C, 10 s) on low energy implanted boron (1 keV) and to achieve depths below 1000 Å. The experiments were done using different partial pressure of oxygen, because of uncertainties in the literature.

The experimental development of process sequences today is very expensive, time- and material-consuming. (In future, with steadily increasing wafer size, experiments are more and more restricted.) The use of advanced process simulation capabilities becomes inevitable, offering the opportunity to immediately visualize and understand physical phenomena which are not easily accessible by experiments [18, 19]. In this contribution, we report the successful implementation of ultra-shallow junction formation simulations based on 1 keV B⁺ implantation and subsequent rapid thermal annealing at 1000°C, 1050°C and 1100°C. The simulations including TED and OED effects are in good agreement with SIMS measurements. The calculations were performed on a workstation using the SSUPREM IV [20] computer code included in the desktop program (framework) Athena [21].

EXPERIMENTAL

The experimental setup is described more precisely by Downey et al. [17]. This short introduction is only focused on the experimental conditions which are relevant for the simulations. N-

type, 200 mm prime Si-wafers, (100)-orientation, 10-20 Ωcm , were used either for ion implantation or to monitor the oxide thickness growth during annealing independent of damaged enhanced oxidation effects [22]. The damage enhancement and the surface properties of these wafers, determined by Scanning Force Microscopy (SFM) measurements, will be discussed in a future publication.

The boron implants (1 keV, dose: $\Phi \approx 1.0 \cdot 10^{15} \text{ cm}^{-2}$) were performed on a Varian VIISion-80 PLUS low-energy high-current implanter at a tilt and twist angle of 0° . The beam current densities have been measured using an in-situ 2D beam profiler. A key issue for these ultra shallow implantations of 400 Å depth is the variability of the native oxide. To avoid any influence prior to the implantation process a 30 s wet-chemical etch was performed in a HF (49%):H₂O (1:40) solution. After implantation a set of two wafers (a bare and an implanted wafer) for each oxygen concentration condition were annealed in a STEAG AST Elektronik SHS2800€ RTP system with Hotliner™ technology. The recipes consist of a prolonged purge step for stabilization of the gas ambient, a prestabilization at 750°C, 10 s, followed by a final 10 s isochronal anneal at 1000°C, 1050°C and 1100°C, respectively, with a ramp up rate of 50 K/s and a 30 K/s ramp down. The standard process technology for shallow junction formation [23] was used only with an adopted gas flow engineering for low oxygen concentration. An average post-anneal uniformity (1σ) of less than 2 % on a 200 mm wafer was found for these ultra-shallow junctions.

The oxygen concentrations during the annealing step in N₂ have been varied in a range of 0-1 ppm to 1 % within this work. For the purpose of these experiments a low-flow oxygen mass flow controller (5 sccm/10 sccm) in conjunction with a standard (30 slm) nitrogen mass flow controller was used to ensure the correct oxygen concentration. The concentration of oxygen was not controlled but sensitively measured/monitored by an ZrO₂/Y₂O₃ ceramic oxygen sensor [24, 25].

The oxide thickness growth within the short annealing time of 10 s is measured using a Plasmos SD3200 single wavelength ($\lambda = 633 \text{ nm}$) ellipsometer (refractive index $n = 1.465$) with a measurement accuracy of 1 Å and a repeatability of 0.1 Å.

Prior to ellipsometric characterization the sheet resistance was probed through the oxide and afterwards all annealed boron implanted wafers were BOE stripped prior to four-point probe measurement on a Prometrix OmniMap RS35c. The implanted profiles have been analyzed using SIMS. The depth profiling was performed at Evans East Inc. using a Physical Electronics Φ 6600 SIMS spectrometer. The near surface concentration accuracy has intentionally been improved by the use of an O-leak technique. The junction depth for the SIMS measurements throughout this publication is defined as the depth where the total concentration, sum of electrical and non-electrical ions falls to a level of $1.0 \cdot 10^{17} \text{ cm}^{-3}$. The SIMS analysis also leads to computational data of the retained dose defined as the ratio of SIMS post-anneal integrated dose and the as-implanted dose.

THEORY AND MODELING

Dopant ion implantation is a critical technology for producing integrated circuits and the correct understanding of the diffusion process is indispensable for the total process flow of the continuously shrinking critical dimensions. The diffusivity of boron, D_B , in silicon is governed by the local concentration of point according to

$$D_B = D_B^I \left(\frac{\langle C_I \rangle}{C_I^*} \right) + D_B^V \left(\frac{\langle C_V \rangle}{C_V^*} \right), \quad (1)$$

where D_B^I and D_B^V are the intrinsic diffusivities due to interaction with self-interstitials, (I), and vacancies, (V), respectively, and $\langle C_X \rangle / C_X^*$ are the local /equilibrium concentration of point defects.

Cowern et al. [26, 27] show that the migration frequency during oxidation-enhanced diffusion is consistent with diffusion-limited kick-out of an interstitial boron species. This information is the physical basis for the computer modeling of the silicon process technology development. Griffin et al. [28] explain their experimental data with a kick-out interstitial boron as mobile species. As present approach, B_i is generated during the changeover of excess silicon self-interstitial atoms, Si_i or I, to substitutional site according to the quasi-chemical reaction (kick-out reaction) [29]



Now that the vacancy contribution to D_B is small or, in other words, that the fractional interstitial component of diffusion, f_I , defined as

$$f_I = \frac{D_B^I}{D_B^V + D_B^I} \quad (3)$$

is close to one [28]. A most reasonable compilation of the Si:B system can be found in [30]. In the present approach the contribution of vacancies is negligible and Eq. (1) simplifies to

$$D_B = D_B^I \left(\frac{\langle C_I \rangle}{C_I^*} \right) = D_B^I \langle S^I \rangle, \quad (4)$$

where $\langle S^I \rangle$ denotes the average I supersaturation due to surface oxidation during Rapid Thermal Annealing. Since the self-interstitial diffusivity D_B^I is very large and the boron penetration depth is extremely shallow, C_I may be considered to be constant over the diffusion zone.

Electronic charge effects cannot be ignored in our simulations because the boron concentration is far above the intrinsic carrier density prevailing at the diffusion temperature (e. g.

$n_i(1050^\circ \text{C}) = 1.97 \cdot 10^{18} \text{ cm}^{-3}$). This implies, that the Fermi level varies over the spatial extent of the diffusion profile. The dependence of the Fermi level effect on the boron diffusion coefficient is modeled using the charged self-interstitial diffusion model in accordance to

$$D_B = D_B^{I,0} + D_B^{I,+} \cdot \left(\frac{p}{n_i} \right) \quad (5)$$

where $D_B^{I,0}$ is the diffusivity via neutral I and $D_B^{I,+}$ the diffusivity via single positively charged I. For the supersaturation of the two self-interstitial species

$$S^I = S^{I,0} = S^{I,+} \quad (6)$$

holds, based on the mass action law.

Since the initial boron profile arises from implantation, Transient Enhanced Diffusion (TED) [31] was taken into account by including an average diffusivity, $\langle D^{TED} \rangle$, in the expression for the effective, extrinsic boron diffusion coefficient, D_B^{eff} , i. e.

$$\begin{aligned} D_B^{eff} &= \langle D^{TED} \rangle + D_B^{I,0} \cdot \langle S^{I,0} \rangle + D_B^{I,+} \cdot \langle S^{I,+} \rangle \cdot \left(\frac{p}{n_i} \right) \\ &= \langle D^{TED} \rangle + \langle S^I \rangle \cdot \left(D_B^{I,0} + D_B^{I,+} \cdot \left(\frac{p}{n_i} \right) \right) \end{aligned} \quad (7)$$

Simulations were performed by using the Fermi method of the SSUPREM IV package. This method makes allowance for the factor p / n_i in Eq. (7) and, in addition, warrants that point defect equilibrium i. e., $C_{I^0} = C_{I^0}^*$ and $C_{I^+} = C_{I^+}^*$, is maintained during diffusion. Furthermore, interactions with vacancies, e. g. I-V-recombination like the Frenkel-Pair mechanism, $I + V \leftrightarrow Si_s$, are excluded a priori. Within this scenario SSUPREM IV simulations yield the following diffusivities for particular oxygen concentrations, pp , in the diffusion ambient:

$$D_{B,pp}^{Sim,0} = \langle D^{TED} \rangle + D_B^{I,0} \langle S_{pp}^I \rangle \quad (8)$$

$$D_{B,pp}^{Sim,+} = D_B^{I,+} \langle S_{pp}^I \rangle \quad (9)$$

It should be emphasized that $D_{B,pp}^{Sim,0}$ and $D_{B,pp}^{Sim,+}$ result from numerical optimization to the SIMS profiles for the various partial pressures of oxygen used, and thus include the effects of transient enhanced diffusion and oxidation enhanced diffusion. The parameters are independently optimized for each SIMS profile. The loss of boron through surface flux (outdiffusion) is taken into account by the standard *TransB*-parameter of SSUPREM IV [21] without any segregation at the Si/SiO₂-interface.

In case of 0-1 ppm of O₂, the so-called *inert diffusion condition*, the enhancement factor $\langle S_{pp}^I \rangle$ equals 1 and $D_{B,pp}^{Sim,+} = D_B^{I,+}$. For all the other partial pressures the enhancement factors are calculated as

$$\langle S_{pp}^I \rangle = \frac{D_{B,pp}^{Sim,+}}{D_B^{I,+}}. \quad (10)$$

Using the set of $\langle S_{pp}^I \rangle$ values thus obtained along with the $D_B^{Sim,0}$ data directly emerging from the simulation, $\langle D^{TED} \rangle$ and $D_B^{I,0}$ result from a linear regression based on Eq. (8).

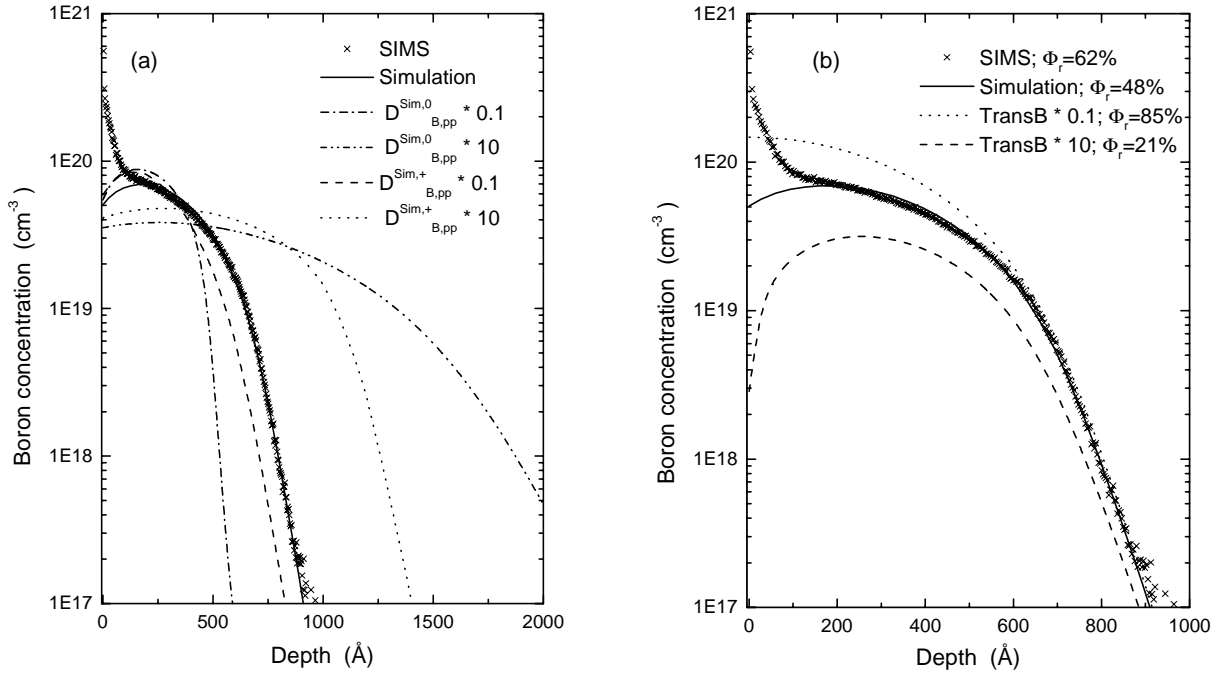


Figure 1: (a) Variation of the $D_{B,pp}^{Sim,0}$, $D_{B,pp}^{Sim,+}$ and (b) $TransB$ for boron diffusion at 100 ppm O₂ and 1050°C 10 s (+) is based on the optimized simulation (solid line) with the following parameter set ($D_{B,pp}^{Sim,0} = 1.43 \cdot 10^{-13} \text{ cm}^2 \text{ s}^{-1}$, $D_{B,pp}^{Sim,+} = 1.38 \cdot 10^{-14} \text{ cm}^2 \text{ s}^{-1}$, $TransB = 6.09 \cdot 10^{-8} \text{ cms}^{-1}$). The differences in retained dose, Φ_r , are mentioned in (b)

In Figure 1 (a) the influence of $D_{B,pp}^{Sim,0}$ and $D_{B,pp}^{Sim,+}$ is illustrated for T=1050°C, $pp = 100$ ppm O₂. $D_{B,pp}^{Sim,0}$ defines the gradient (steepness) of the profile in the lower concentration regime and $D_{B,pp}^{Sim,+}$ changes the depth (junction) evidently depending on the extrinsic doping level (see Eq. (5), (7)). The shape of the profile is determined by the ratio $R = D_{B,pp}^{Sim,0} / D_{B,pp}^{Sim,+}$. For very large values of R the profile becomes *erfc*-like. In contrast for small R values a rather box-like shape

arises due to the concentration dependent factor p / n_i in Eq. (7). In Figure 1 (b) the outdiffusion of boron is varied by the $TransB$ -parameter. An increasing flux leads to a decrease of the total boron concentration near the surface. For effectively small $TransB$ values the surface flux is negligible, no dopant-loss occurs, and for $x = 0$ nearly the solid solubility for this temperature is reached.

RESULTS AND DISCUSSION

As-implanted profiles

A complete simulation of the entire process sequence including both, the implantation and rapid thermal annealing processes, is essential.

Before simulating the time and temperature dependence of profile broadening, the as-implanted $^{11}\text{B}^+$ distribution has to be matched.

The good agreement of simulated and experimental data in Figure 2 clearly shows, that analytical models are sufficient for the simulation of the implantation process. In contrary to more complex Monte-Carlo based calculations [32], providing a detailed damage and recoil distribution but also requiring an enormous modeling and program execution effort, the implanted profiles were constructed from a previously prepared set of parameters. A simple Gaussian distribution modeling of the implanted profiles turned out to be inadequate. For the calculation of the asymmetric profiles, a widely approved Pearson IV distribution was assumed [33]. This is the only type of function having a single maximum and a monotonous decay to zero on both sides of the distribution.

To account for the pronounced tail, which is observed in the SIMS profiles of the as-implanted sample, a dual Pearson method was applied. The implant concentration is calcu-

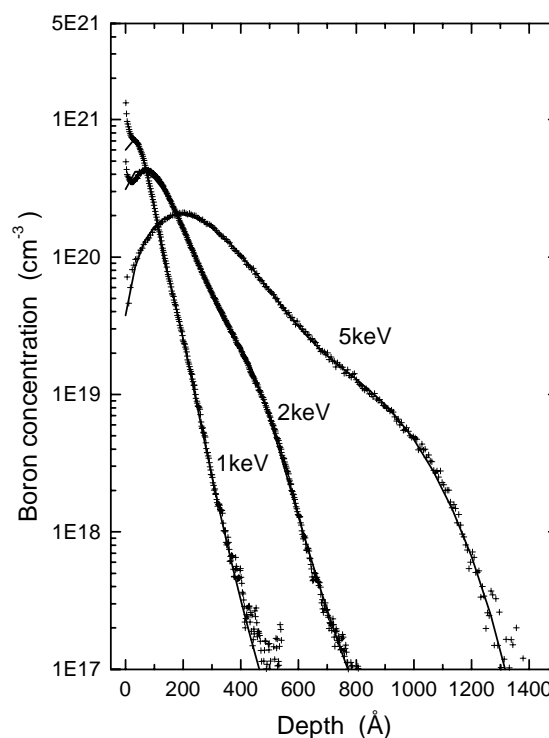


Figure 2: SIMS profiles of the as-implanted boron distribution for 1 keV, 2 keV and 5 keV. The solid lines denote the simulation results with the parameter summarized in Table I

lated as a linear combination of two Pearson distributions, each with its own set of moments

$$C(x) = [\Phi_1 \cdot f_1(x) + \Phi_2 \cdot f_2(x)] = \Phi \cdot [\mathfrak{R} \cdot f_1(x) + (1 - \mathfrak{R}) \cdot f_2(x)], \quad (11)$$

where Φ is the total implantation dose, Φ_1 denotes the fraction covered by the random scattering part around the peak of the profile and Φ_2 represents the dose fraction covering the channeling tail region. Existing material data are only available above 5 keV. For implantation energies below 5 keV a set of range parameters has previously been calculated by interpolation of existing, experimentally verified 5 and 0.5 keV data for implants into a bare Si surface without any native oxide layer. However, low energy implants have been reported to be extremely sensitive to the presence of ultra-thin native oxide layers [34]. Hence, accurate simulation of OED has to include the simulation of the oxidation process. Up to now, there is no experimental verification of the model for boron below 5 keV.

Table I: Parameter set for the simulation of reduced energy implants (1 to 5 keV) for ultra-shallow junction formation. A dual Pearson implant model and numerical optimization techniques were used to calibrate the model with the SIMS Profiles shown in Figure 2

Parameter	1 keV B implant	2 keV B implant	5 keV B implant
dose, Φ , (cm^{-2})	$6.73 \cdot 10^{14}$	$8.13 \cdot 10^{14}$	$8.02 \cdot 10^{14}$
energy (keV)	1.0	2.0	5.0
tilt angle ($^\circ$)	0	0	0
R_{p1} (nm), 1 st Pearson	1.68	10.3	24.7
ΔR_{p1} (nm), Std. Dev.	3.28	8.02	14.4
skewness, 3 rd moment	0.62	0.74	0.64
kurtosis, 4 th moment	2.52	3.16	3.18
R_{p2} (nm), 2 nd Pearson	7.71	36.6	63.9
ΔR_{p2} (nm) Std. Dev.	7.09	11.1	22.8
skewness, 3 rd moment	0.28	-0.32	-0.028
kurtosis, 4 th moment	4.84	8.72	2.77
$\mathfrak{R} = \Phi_1 / (\Phi_1 + \Phi_2)$	0.67	0.94	0.89

The high near-surface concentration peak for both, as-implanted and diffused SIMS profiles, must be attributed to the well-known SIMS knock-on effect (tracing and secondary ion implantation by the oxygen sputter beam used for SIMS analysis). Although the measured boron concentrations strongly exceed the solubility limit of boron in silicon under equilibrium conditions in

this area, a significant disadvantageous impact has not been observed. A similar increased concentration is observed for the as-implanted boron profiles for acceleration energies of 1 keV to 5 keV. The calibration of the parameter set was done by numerical optimization. The determined parameter sets had to be corrected in agreement with other data with respect to reduced projected range values. Special adaptations were necessary for the third and fourth moments (skewness and kurtosis, respectively) to account for the pronounced tail. For the very low acceleration energies the impact of the tilt angle on the channeling behavior is negligible. A decrease in the projected range values R_{p1} and R_{p2} is observed for both peaks, the 1st and 2nd Pearson distribution, with reduced implantation energies.

The reduction in the acceleration energies has almost no impact on the standard deviation, ΔR_{p1} , of the 1st Pearson distribution, but a pronounced influence on the standard deviation, ΔR_{p2} , of the 2nd peak distribution, which accounts for the increasing channeling effects. The high ratio, \mathfrak{R} , of the dose Φ_1 , describing random scattering with respect to the overall dose $\Phi = \Phi_1 + \Phi_2$, indicates that the concentration profile is mainly influenced by the 1st Pearson distribution, whereas the importance of the 2nd peak distribution, determining the tail of the implanted profiles, gains of importance for reduced implantation energies. The implemented parameter set is summarized in Table I.

Post RTA profiles

The gaseous ambient during rapid thermal annealing plays a crucial role for ultra-shallow junction formation. The temperature and the oxygen partial pressure were varied in the experiments, whereas the annealing time for low-energy boron implants was set to 10 s (standard value, often given in literature). In Figure 3, the dependence of the oxide thickness on the partial pressure is displayed. Beginning from 33 ppm a monotonous increase of the oxide thickness, t_{ox} , with the O_2 concentration is visible. Even the variation of small oxygen concentrations leads to measurable dif-

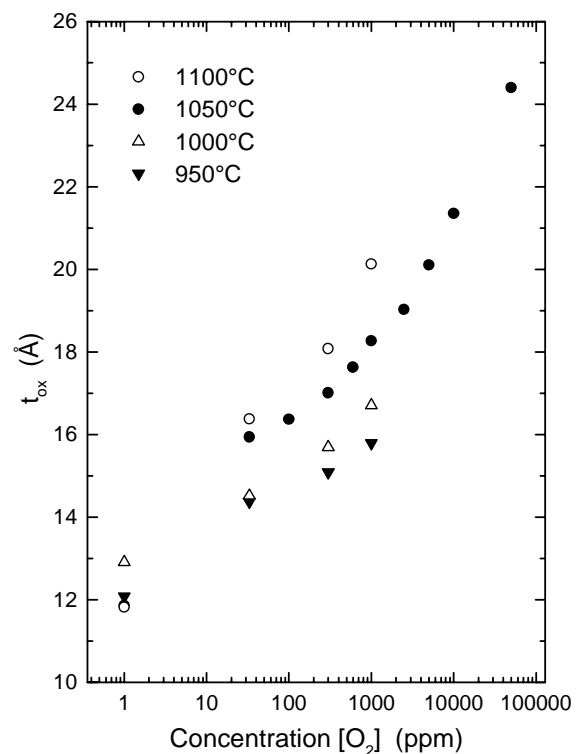


Figure 3: Oxide thickness, t_{ox} , versus oxygen concentration, $p(O_2)$, for 1000°C, 1050°C, 1100°C and isochronal annealing condition (10s)

ferences in the oxygen growth during annealing. For 0-1 ppm, visible etching of the wafer surface occurs at 1000°C, 1050°C and 1100°C. The measured oxide thickness is slightly thinner than the native oxide thicknesses of wafers from the same batch [35, 36, 37].

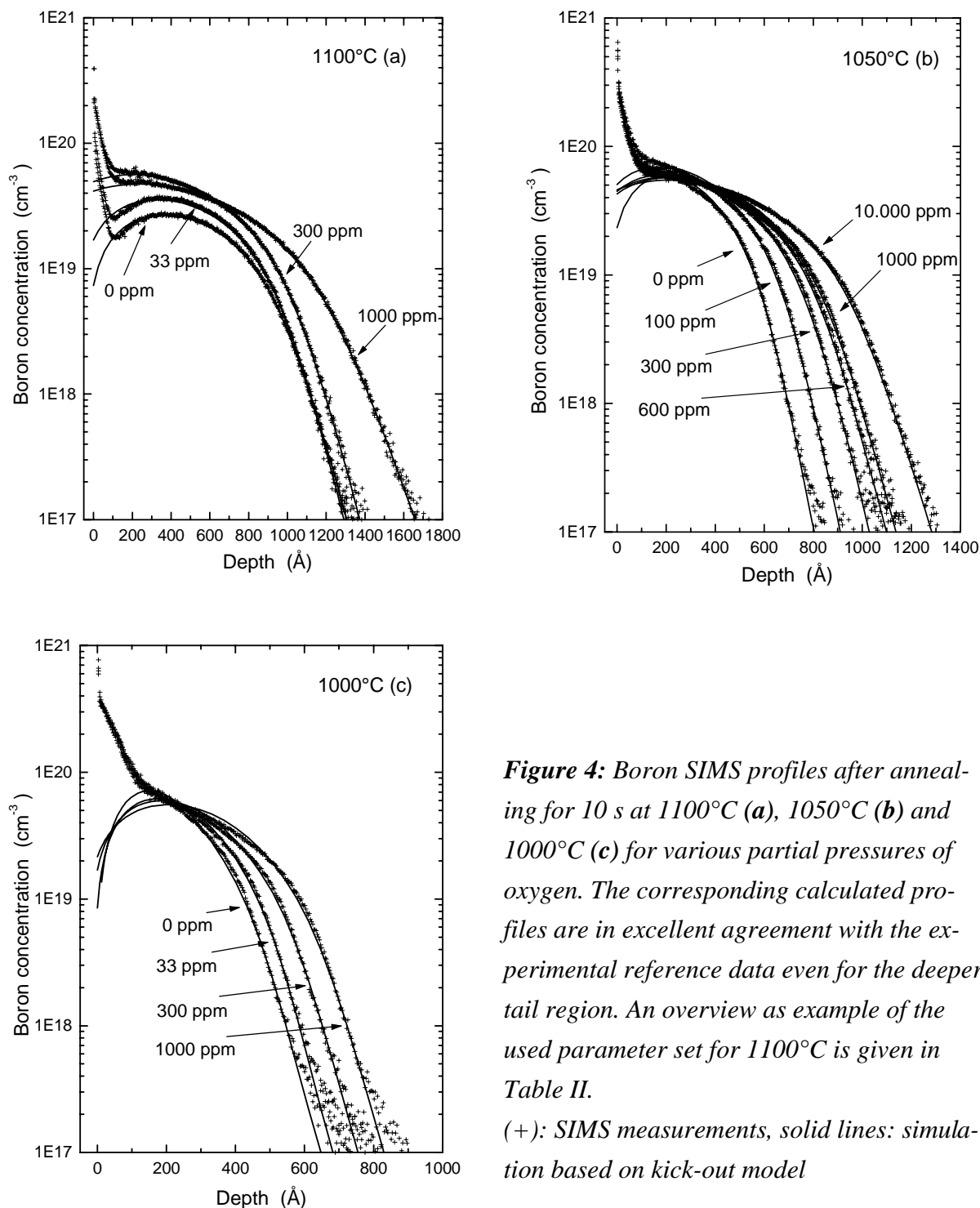


Figure 4: Boron SIMS profiles after annealing for 10 s at 1100°C (a), 1050°C (b) and 1000°C (c) for various partial pressures of oxygen. The corresponding calculated profiles are in excellent agreement with the experimental reference data even for the deeper tail region. An overview as example of the used parameter set for 1100°C is given in Table II. (+): SIMS measurements, solid lines: simulation based on kick-out model

Comparably grown oxides on bare silicon wafers were checked by XPS (X-ray Photoelectron

Spectroscopy) but no suboxides (SiO_x , $x < 2$) were found for this time regime [38]. The starting of the surface oxidation (> 33 ppm) is accompanied by the generation of excess silicon self-interstitials at the interface migrating into the bulk and leading to a diffusion enhancement [39].

In Figure 4 (a, b, c) boron concentration profiles measured by SIMS are displayed together with the numerically simulated curves. The simulations displayed by the solid curves are in excellent agreement with experimental data. It is obvious, that for all annealing temperatures the junction depth decreases monotonically, i. e. for 1050°C from 1290 \AA to 820 \AA with decreasing O_2 -concentration from 1 % down to 33 ppm. The shallowest junction is deduced from the simulations at 1000°C with a concentration of 100 ppm O_2 and has a depth of 755 \AA . The equivalent junction at 1100°C is 1380 \AA deep.

In the literature [40], some differences between experimental and simulated data are reported when using SSUPREM IV without additional calibrations for ultra-low energy boron implantations. Our successful implementation of the diffusion simulation confirms the consequently adopted model. Also our initial attempts to fit the measured boron profiles with the SSUPREM IV default parameter set for oxidizing ambient was not successful. This indicates, that the standard SSUPREM IV extrapolation to conditions of extremely low energy, high dose implantation and RTA under oxidizing ambient is not a valid approach. Therefore, we have chosen an alternative strategy in which relevant information about OED and TED in this extreme regime of Si:B processing is extracted from a simplified simulation model, as outlined in the preceding section. This strategy has led to excellent adjustments of the experimental profiles, i. e., by using the parameters listed in Table II.

Table II: Parameter set for the simulation of the diffusion of 1 keV boron implant (1050°C , 10s) at four different partial pressures for the formation of ultra-shallow junctions

Parameter	0 ppm	33 ppm	300 ppm	1000 ppm
$D_{B,pp}^{Sim,0} \text{ (cm}^2\text{s}^{-1}\text{)}$	$1.12 \cdot 10^{-13}$	$1.10 \cdot 10^{-13}$	$1.93 \cdot 10^{-13}$	$2.42 \cdot 10^{-13}$
$D_{B,pp}^{Sim,+} \text{ (cm}^2\text{s}^{-1}\text{)}$	$7.98 \cdot 10^{-15}$	$7.72 \cdot 10^{-15}$	$1.91 \cdot 10^{-14}$	$2.50 \cdot 10^{-14}$
$TransB \text{ (cms}^{-1}\text{)}$	$1,29 \cdot 10^{-7}$	$6.43 \cdot 10^{-8}$	$6.65 \cdot 10^{-8}$	$6.24 \cdot 10^{-8}$

All profiles with 0 and 33 ppm at the various temperatures show anomalous behaviour. To account for this effect, the outdiffusion parameter for these profiles is set to higher values compared to the ones annealed with higher oxygen concentrations.

The optimized diffusion coefficients are slightly higher than the ones for 33 ppm. This phenomenon results from the etching of the wafer surface during annealing and can be explained by the movement of the SiO₂-surface plane. The etching slowly reduces with increasing oxygen concentration and decreasing annealing temperatures and is absent below 1000°C. SFM measurements reveal the SiO etching [17, 36]. For bare silicon wafers (process: 1150°C, 30s) without implantation, the etching occurs up to 250 ppm of oxygen and decreases in strength with increasing oxygen concentration. 500 ppm shows an absolute smooth surface [36].

The limiting factor for ultra-shallow junction therefore is the controlled O₂-concentration during annealing. Undetected O₂-back-ground concentration levels in rapid thermal annealing systems lead to unintentional broadening of the as-implanted condition as reported by others [16] but can on the other hand also destroy a junction due to etching.

The high concentration profile peak from the surface up to 100 Å is most probably due to the well known SIMS knock-on effect because the solubility limit of boron in silicon is strongly exceeded in this area. A similar higher concentration is obvious at the as-implanted boron profiles for 1 keV to 5 keV (Figure 2).

The retained dose, Φ_r , being the integrated boron concentration after annealing as percentage of the implanted dose, shows marked differences for the simulated profiles compared to the SIMS profiles. This effect is displayed for example in Figure 5 for the 1050°C data. There is a constant offset for the whole oxygen partial pressures of 12 %, which supports the view that the boron surface peak originates from SIMS artifacts. However the high boron concentration at the Si/SiO₂ interface or in the SiO₂ due to outdiffusion may lead to back-tracing of boron atoms during the SIMS measurement. Also a formation of a silicon boride phase (SiB₄) at boron concentrations higher than 6% may be possible [16]. TOF-SIMS (Time Of Flight SIMS) measurements could yield a better understanding of this artifact in the

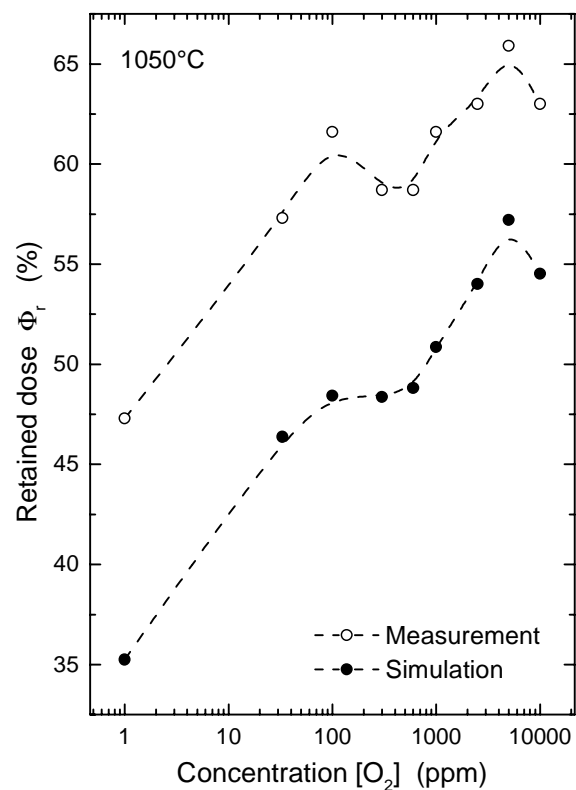


Figure 5: The simulated and measured retained dose is displayed for 1050°C. The increase with oxygen concentration is obvious. Open symbols: deduced from SIMS measurement; closed ones: from simulations

first 10 nm of the profiles. Under production conditions, the simulated profiles reflect the real situation of outdiffusion/dopant loss. The measured as well as the simulated data show a distinct increase with the oxygen concentration and saturate at a value of around 60 %.

The user can find an optimum annealing condition for his sub-0.18 μm process from our simulations together with the more detailed data collection/interpretation of Downey et al. [17]. It is up to the user to weigh the advantages and the disadvantages.

The analysis of the above SIMS profiles leads to values of silicon self-interstitial supersaturations for isochronal/isothermal annealing conditions in different oxidizing ambients. In Figure 6, the deduced S_{pp}^I data are displayed as a function of the temperature and partial pressure of oxygen. The $S_{pp}^I = 1$ data point is the same for all temperatures and describes the *inert annealing condition* (0-1 ppm of oxygen). The tendency of increasing supersaturation with increasing partial pressure and decreasing temperature can be explained based on the circumstance that C_I^* decreases with temperature [41]. In case of 1100°C annealing, only slight excess concentrations of self-interstitials ($S_{pp}^I < 1.5$) occur and the crystal is in thermal equilibrium during the short annealing cycle of 10 s. At 1000°C and 1050°C a non-equilibrium concentration is generated in the crystal leading to diffusivity enhancement of the dopant atoms. Antoniadis et al. examined OED of boron under near-intrinsic conditions. Their data indicate that the diffusivity enhancement during dry oxidation range from a factor of 100 at 850°C to a factor of 1.2 at 1100°C in $\langle 100 \rangle$ silicon [42]. Retarded diffusion was not observed at any temperature. The data in Figure 6 are therefore in fairly good agreement with the literature.

In the following, latest RTA data are compared with existing literature data mainly deduced from furnace annealing [31, 42, 43].

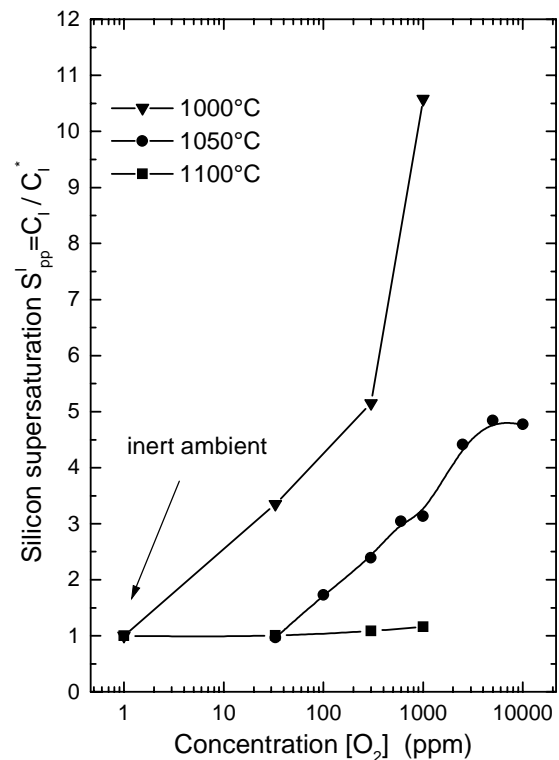


Figure 6: The enhancement factor versus oxygen concentration for 1000°C, 1050°C and 1150°C. The solid lines are not based on a model but for guiding the eye only

In Figure 7 the extracted B diffusion coefficients due to neutral and positively-charged self-interstitials and values for the transient enhanced diffusion coefficient are displayed. The agreement of $D_B^{I,0}$ with data from Antoniadis et al. [42] and from Fair [43], who separated the diffusion coefficient in a charge-dependent and a neutral one by reviewing and evaluating literature [30], is satisfactory apart from the data point at 1000°C. The Arrhenius relationship of Fair for $D_B^{I,+} + D_B^{I,0}$ almost coincides with that of Antoniadis et al. Our data are from short-time diffusion annealings, whereas the other authors used conventional furnace technology. The contribution of $D_B^{I,+}$ extracted from our experiments to the sum, $D_B^{I,+} + D_B^{I,0}$ is rather small. The Arrhenius relationship for $D_B^{I,+}$ is much steeper compared to the diffusion via the neutral species. But the influence of $D_B^{I,+}$ is enhanced via the self-doping factor p/n_i .

The present $\langle D^{TED} \rangle$ value in Figure 7 is only a weak function of temperature and appreciably smaller than the data from Solmi et al. (e.g. $6.59 \cdot 10^{-12} \text{ cm}^2\text{s}^{-1}$ at 1050°C) [31]. These data were extracted from SSUPREM III simulations with a satisfactory agreement between SIMS measurement and calculated profile. Mainly the tail region shows some deviations. Furthermore, the dose varies between $2.0 \cdot 10^{14} \text{ cm}^{-2}$ and $5.0 \cdot 10^{15} \text{ cm}^{-2}$ while the energy is 20 to 30 times higher compared to that in the present work. Solmi et al. state, that the reduction of the projected range is expected to lead to smaller $\langle D^{TED} \rangle$ values. The influence depends strongly on the annealing temperature and time [31]. The present 1 keV boron implantation is thus expected to produce a smaller TED effect because of the reduced damage involved. Nevertheless, the effect is strong enough to have an important impact on the boron diffusion coefficient i. e. via the silicon self-interstitial supersaturation, especially at 1000°C due to generated I from implant damage.

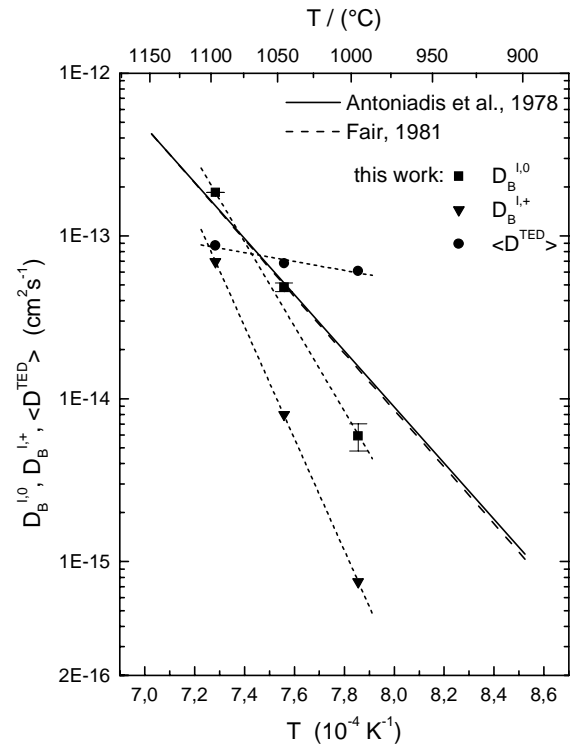


Figure 7: Diffusions coefficients of boron deduced from the present data and compared to Arrhenius relationships from the literature (solid line: Antoniadis et al. [42], intrinsic non oxidizing ambient; dashed line: Fair [43], intrinsic diffusion via $D_B^{I,0}, D_B^{I,+}$:

$$D_B^{I,+} + D_B^{I,0} \approx D_B^{I,+} (\text{Fair})$$

Agarwal et al. show reduced TED with decreasing implantation energy and dose for rapid thermal annealing. For the same energy (1keV) and a factor of 10 higher dose ($\Phi = 1.0 \cdot 10^{15} \text{ cm}^{-2}$) compared to the smallest TED, a significant increase in enhancement is observed. The minimum enhancement (factor ≈ 4 , cf. Fig. 6) is independent of decreasing energy and named Boron-Enhanced-Diffusion.

Our data show a smaller TED effect compared to Solmi et al. and a slightly smaller one to Agarwal et al. The lack of detailed information on the exact environmental process condition in [16] and the agreement with our 1000 ppm data let us assume that the authors can not separate the superimposing/competing effect of TED via implantation defects and the enhancement of the boron diffusivity via OED by an surface oxidation with injection of excess silicon self-interstitials. In the literature, only few authors reported their gas ambients during annealing to be absolutely pure nitrogen [15, 45, 46] or control their ambient during annealing with a oxygen sensor [17].

After this first global approach to ultra-shallow junction simulation a more basic description should include the injection of I generated at the SiO_2/Si -interface into the bulk and the reflux of self-interstitials from the bulk into the oxide [47]. Furthermore, a more precise model for boron outdiffusion is necessary. On the other hand, for a better understanding of the mechanism involved, isothermal experiments at one partial pressure would provide a more extensive data base.

SUMMARY

Parameters that produce significant effects on junction depth are annealing ambient, especially the O_2 concentration, as well as annealing time and temperature. The improved O_2 ambient control in the STEAG AST SHS2800 ϵ RTP system enables the formation of ultra-shallow junctions and thus meets the challenging requirements of future CMOS device and circuit generations to minimize short channel effects and improve the subthreshold behavior. The very good agreement of simulated and experimental data confirms the successful implementation of the whole process sequence for ultra-shallow junctions formation, which consists of a low energy implantation process and a subsequent rapid thermal anneal. From our experiments we deduced the silicon self-interstitial supersaturation as function of oxygen concentration (0-1,....,10000 ppm) and temperature (1000°C, 1050°C, 1100°C). Additionally, boron diffusion coefficients determined from the simulations relate to interactions of B with neutral and positively charged self-interstitials on the one hand and to TED on the other hand. In conclusion, the used process simulators have emerged as powerful tools for effective process development.

ACKNOWLEDGMENTS

The authors would like to thank Dr. G. Roters for helpful discussions and critical reading of the manuscript. Special thanks to Dr. Z. Nenyeyi, A. Tillmann, the Applications Lab staff of STEAG AST Elektronik GmbH and the VARIAN IIS team, including co-authors of our previous communications.

REFERENCES

- [1] F. Roozeboom in Advances in Rapid Thermal and Integrated Processing, edited by F. Roozeboom, NATO ASI Series E, Vol. 318, (Kluwer Academic Publ. 1996)
- [2] D. F. Downey, S. L. Darayanani, M. Meloni, K. Brown, S. B. Felch, B. S. Lee, S. D. Marcus, J. C. Gelpey
Mat. Res. Soc. Symp. Proc. **470** 299-311 (1997)
- [3] D. F. Downey, C. M. Osburn, S. Marcus
Solid State Technology No. **12/97** 71-82 (1997)
- [4] S. D. Marcus, D. F. Downey, S. L. Darayanani, J. W. Chow
Proc. 5th Int. Conf. on Advanced Thermal Processing-RTP'97 64-71 (1997)
- [5] C. M. Osburn, D. F. Downey, S. B. Felch, B. S. Lee
Proc. 11th Int. Conf. on Ion Implantation Technology 67-74 (1997)
- [6] C. M. Magee, J. Shallenberger, M. Denker, D. F. Downey, M. Meloni, S. Clotherty, S. B. Felch
Proc. 4th Intl. Workshop on Ultra-Shallow Junctions p. 8.1 (April 1997)
- [7] D. F. Downey, U.S. Patent pending application
Methods for forming shallow junctions in semiconductor wafers using controlled low level oxygen ambient during annealing (1998)
- [8] Semiconductor Industry Association (SIA)
National Technology Roadmap for Semiconductors, Stevens Creek Blvd., Suite 271, San José (CA) 1997
- [9] A. D. Lilak, S. K. Earles, K. S. Jones, M. E. Law, M. D. Giles
IEEE Tech. Dig. IEDM'97, 493-496, Washington, Dec. 1997
- [10] S. S. Yu, H. W. Kennel, M. D. Giles, P. A. Packan
IEEE Tech. Dig. IEDM'97, 509-512, Washington, Dec. 1997
- [11] S. M. Hu
Appl. Phys. Lett. **43**(5) 449-451 (1983)
- [12] S. M. Hu
J. Electrochem. Soc. **139**(7) 2066-2075 (1992)

- [13] H. S. Chao, P. B. Griffin, J. D. Plummer, C. S. Rafferty,
Appl. Phys. Lett., **69** 2113-2115 (1996)
- [14] D. J. Eaglesham, P. A. Stolk, H.-J. Gossmann, J. M. Poate
Appl. Phys. Lett. **65** 2305-2307 (1994)
- [15] N. E. B. Cowern, G. F. A. van de Walle, P. C. Zalm, D. W. E. Vandenhoudt
Appl. Phys. Lett. **65**(23) 2981-2983 (1994)
- [16] A. Agarwal, D. J. Eaglesham, H.-J. Gossmann, L. Pelaz, S. B. Herner,
D. C. Jacobson, T. E. Haynes, Y. Erokhin, R. Simonton
IEEE Tech. Dig. IEDM'97, 467-470, Washington, Dec. 1997
- [17] D. F. Downey, J. W. Chow, W. Lerch, J. Nieß, S. D. Marcus
The Effects of Small Concentrations of Oxygen in RTP Annealing of Low Energy Boron,
BF₂ and Arsenic Ion Implants
to be presented at MRS April 1998, and published in the MRS RTP Proceeding
- [18] H. Walk, M. Schäfer, M. Glück, U. König
Solid State Technology No. **3/97** 16-18 (1997)
- [19] M. Glück, D. Behammer, M. Schäfer, H. Walk, U. König
Proc. of SISPAD'97, 197-200, 8.-10.9.1997, Cambridge (MA)
- [20] Computer code SSUPREM IV developed at the Integrated Circuits Laboratory Stanford
University by R. W. Dutton and J. D. Plummer
- [21] ATHENA is a trademarked and commercially available process simulation framework
developed by SILVACO International comprising SSUPREM IV
- [22] J. F. Götzlich, K. Haberer, H. Ryssel
Gordon and Breach Science Publishers Inc. 203-209 (1980)
- [23] W. Lerch
phys. stat. sol. (a) **158** 117-136 (1996)
- [24] R. Mader, private communications,
- [25] S. Marcus, W. Lerch, D. F. Downey, S. Todorow, J. Chow
RTP Requirements to yield uniform and repeatable Ultra-Shallow Junctions with low en-
ergy Boron and BF₂ ion implants
presented at 127th Annual Meeting & Exhibition of the TMS 1998, 15. - 17. Feb. 1998
San Antonio (TX), to be published in J. of El. Mat. June/July (1998)
- [26] N. E. B. Cowern, K. T. F. Janssen, G. F. A. van de Walle, D. J. Gravesteijn
Phys. Rev. **65**(19) 2434-2437 (1990)
- [27] N. E. B. Cowern, G. F. A. van de Walle, P. C. Zalm, D. J. Oostra
Phys. Rev. **69**(1) 116-119 (1992)

- [28] P. B. Griffin, R. F. Lever, P. A. Packan, J. D. Plummer
Appl. Phys. Lett. **64**(19) 1242-1244 (1994)
- [29] U. Gösele, W. Frank, A. Seeger
Appl. Phys. **23** 361-368 (1980)
- [30] Landolt-Börnstein: New Series III/**33A** , Group III: Condensed Matter
Diffusion in Semiconductors and Non-Metallic Solids
Subvolume A, Diffusion in Semiconductors, ed. by D. L. Beke
(Springer, Berlin) 1998
- [31] S. Solmi, F. Baruffaldi, R. Canteri
J. Appl. Phys. **69**(4) 2135-2142 (1991)
- [32] G. Hobler, H.-H. Vuong, J. Bevk, A. Agarwal, H.-J. Gossmann, D. C. Jacobson,
M. Foad, A. Murrell, Y. Erokhin
IEEE Tech. Dig. IEDM'97, 489-492, Washington, Dec. 1997
- [33] S. M. Sze, VLSI Technology, 2nd Edition,
(McGraw-Hill International Editions, 1988), pp. 332-340
- [34] K. B. Parab, D. H. Hang, S. J. Morris, S. Tian, A. F. Tasch, D. Kamenitsa, R. Simonton,
C. Magee
J. Vac. Sci. Technol. **B14**(1) 260-264 (1996)
- [35] Z. Nenyeyi, S. Sommer, J. Gelpey, A. Bauer
Mater. Res. Soc. Proc. **342** 401-406 (1994)
- [36] Z. Nenyeyi, G. Wein, W. Lerch, C. Grunwald, J. Gelpey, S. Wallmüller
Proc. 5th Int. Conf. on Advanced Thermal Processing-RTP'97, 35-44 (1997)
- [37] F. W. Smith, G. D. Ghidini
J. Electrochem. Soc. **129**(6) 1300-1306 (1982)
- [38] Z. Nenyeyi, K. Rührschopf
private communications, 1998
- [39] P. M. Fahey, P. B. Griffin, J. D. Plummer
Rev. Mod. Phys. **61**(2) 289-384 (1989)
- [40] R. P. Webb, M. A. Foad, R. M. Gwilliam, A. P. Knights, G. Thomas
Mat. Res. Soc. Proc. **469** 59-63 (1997)
- [41] H. Bracht, N. A. Stolwijk, H. Mehrer
Phys. Rev. **B52** 16542-16550 (1995)
- [42] D. A. Antoniadis, A. G. Gonzalez, R. W. Dutton
J. Electrochem. Soc. **125**(5) 813-819 (1978)
- [43] R. B. Fair, in Impurity Doping, edited by F. F. Y. Wang
(North Holland Publishing Company, Amsterdam, North Holland) pp. 315-442 (1981)

- [44] J. M. Paote, D. J. Eaglesham, G. H. Gilmer, H.-J. Gossmann, M. Jaraiz, C. S. Rafferty, P. A. Stolk
IEEE Tech. Dig. IEDM'95, 77-80, Washington, Dec. 1995
- [45] L. H. Zhang, K. S. Jones, P. H. Chi, D. S. Simons
Appl. Phys. Lett. **67**(14) 2025-2027 (1995)
- [46] A. E. Michel, W. Rausch, P. A. Ronsheim, R. H. Kastl
Appl. Phys. Lett. **50**(7) 416-418 (1987)
- [47] W. Lerch, N. A. Stolwijk
J. Appl. Phys. **83**(3) 1312-1320 (1998)